Out-of-plane magnetoresistance in ferromagnet/graphene/ferromagnet spin-valve junctions

Jae-Hyun Park and Hu-Jong Lee
Department of Physics, Pohang University of Science and Technology, Pohang 790-784, Republic of Korea
(Received 28 January 2014; revised manuscript received 30 March 2014; published 21 April 2014)

Out-of-plane spin-injection and detection through naturally stacked graphene layers were investigated in ferromagnet/graphene/ferromagnet (FGF) junctions. We obtained a maximum magnetoresistance (MR) of 4.6% at $T = 4.2$ K in the junction of a four-layer graphene insertion, having a very small area−junction-resistance product of 0.2 $\Omega\,\mu\text{m}^2$. According to resistance-temperature and current-voltage characteristics, the graphene layer in the FGF junction acted as a metal-like insertion rather than as an insulating barrier. A lower value for the interfacial spin asymmetry coefficient ($\gamma = 0.25 \pm 0.05$) obtained from the fitting of variations with interfacial resistance implies that the spin-injection efficiency along the out-of-plane direction was reduced by spin-flip scattering at graphene/ferromagnet interfaces. Our results showed that highly transparent graphene/ferromagnet interfaces with crystalline ferromagnet (FM) electrodes are required to achieve higher spin-injection efficiency through the graphene layer in a FGF junction along the out-of-plane direction.

DOI: 10.1103/PhysRevB.89.165417 PACS number(s): 75.76.+j, 72.80.Vp, 72.25.Mk, 85.75.−d

I. INTRODUCTION

Persistent in-plane propagation of spin-polarized carriers in graphene without spin flips has been predicted as a result of its weak spin-orbit scattering and weak hyperfine coupling. However, this prediction has not been experimentally realized due to intrinsic scattering (i.e., spin precession via internal spin-orbit fields) or extrinsic scattering (i.e., impurity scattering in graphene) [1–7]. To minimize attenuation of the spin polarization of carriers during transmission along the in-plane direction, the graphene in contact with the disorder-free ferromagnetic electrodes must be exceptionally clean and ultraflat [8–11].

Similar to in-plane spin injection into graphene, out-of-plane ferromagnet/graphene/ferromagnet (FGF) junctions realized by utilizing the crystallinity of naturally stacked graphene layers are also considered promising for achieving highly persistent spin polarization of carriers during transmission between the ferromagnetic injector and detector electrodes [12–14]. This is attributed to the graphene-layer thickness, which is much shorter than the characteristic spin-flip scattering length along the out-of-plane direction. The spin-flip length reaches ∼100 nm in graphite for hot carriers (1.8 eV above the Fermi level) [15] while it is a few tens of nm in organic semiconductors for normal carriers [16–18]. High transmission of spin-polarized hot carriers along the out-of-plane direction of weakly bonded graphene sheets (7–17 nm thick) has been observed via ballistic electron magnetic microscopy [15]. Optimization of the spin efficiency in FGF junctions requires precise control over the graphene/FM interfacial characteristics.

Recently, a few observations have been made using graphene layers grown by chemical vapor deposition (CVD) as insertion layers in FGF junctions [19–21]. It was shown that single-layer graphene acts as an insulating barrier, as in magnetic tunnel junctions, showing magnetoresistance (MR) of 2% at $T = 4.2$ K in NiFe/graphene/Co junctions [19] with the value of the AR product of 35 and 75 $\text{k}\Omega\,\mu\text{m}^2$ (A and R are the area and resistance of the FGF junctions, respectively). By contrast, single-layer graphene in FGF junctions, with smaller AR products of 40 $\Omega\,\mu\text{m}^2$ in Ref. [20] (NiFe/graphene/NiFe) and a few $\text{k}\Omega\,\mu\text{m}^2$ in Ref. [21] (Co/graphene/Co), acted as a metallic insertion between two FM electrodes, showing MR of 0.15% and 1.0%, respectively. In these experiments, the bottom FM electrodes were attached by transferring the CVD-grown graphene layers onto predeposited FM electrodes. This process may have resulted in the degradation of the bottom FM electrodes due to extended direct exposure to air, leading to suppression of magnetoresistance (MR).

It has been theoretically proposed [12–14] that highly effective spin filtering is attainable along the c-axis crystal direction at the interface between graphene and crystalline Ni or Co electrodes; this is due to the minor lattice mismatch (1.3%) and electronic-structure overlap in reciprocal space exclusively for minority spins. The spin filtering is predicted to be enhanced for larger number of atomic layers in a graphene stack. In followup measurements in Ni/graphene/Al_2O_3/Co junctions with graphene grown by CVD directly on a Ni electrode, a negative MR was observed, which was attributed to the theoretically predicted spin-filtering effect at the Ni/graphene interface [22]. However, FGF junctions prepared by sandwiching double-layer graphene, i.e., two pieces of single-layer graphene physically stacked together, between two FM electrodes showed low MR of 0.5% in Ref. [20] and of 1.0% in Ref. [21].

Here, we present our results for the out-of-plane spin-valve effect in FGF junctions using naturally stacked graphene with a varied number of layers. Because the spin-filtering effect has been predicted to be effective for multiple-layer graphene, we examined the variation of MR with respect to the number of graphene layers. The "flip-transfer" method, developed recently by our group [23], was adopted to sandwich graphene layers between two permalloy (Py; $Ni_{0.81}Fe_{0.19}$) electrodes. This technique prevented the degradation of the surface of the bottom Py electrode from air exposure or chemicals during the nanofabrication process, which led to very small interfacial resistance AR_{cont} in our junctions (see Table I). The maximum MR of 4.6% was observed at $T = 4.2$ K in a FGF junction with a four-layer-graphene insertion, which is the highest among those obtained from graphene-based spin-valve devices. In our

TABLE I. Junction parameters: the number of graphene layers, lateral dimension of junctions, resistance at $T = 4.2$ K, AR_{cont}, magnetoresistance (MR), and type of junctions, according to their temperature dependence of resistance.

Sample	Number of layers	Length (μm)	Width (μm)	R_{jnc} (Ω)	AR_{cont} ($\Omega\,\mu m^2$)	MR (%)	Type of junction
G1-t	1	4.55	0.75	0.118	0.188	2.73	Transparent
G1-r	1	4.15	0.61	1.280	1.620	0.31	Resistive
G2-t	2	4.49	0.70	0.252	0.392	2.80	Transparent
G2-r	2	4.48	0.73	0.553	2.828	0.70	Resistive
G3-r	3	4.52	0.87	0.474	0.943	2.02	Resistive
G4-t	4	4.42	0.77	0.057	0.093	4.58	Transparent
G4-r1	4	4.42	0.77	0.073	0.123	2.28	Resistive
G4-r2	4	4.66	0.86	0.736	1.461	1.30	Resistive

devices, the graphene layers acted as a metal-like insertion, as evidenced by the weak temperature dependence of zero-field resistance and MR, and the bias insensitivity of MR. The higher MR observed for our FGF junctions with smaller AR_{cont} indicated that spin flips occurred mainly at the graphene/Py interfaces and that a clean interface is required for high spin injection. However, the theoretically predicted spin filtering effect was not observed in our FGF junctions, presumably because the lattice matching between the graphene layer and the amorphous (crystalline) Py electrodes was not realized.

II. FABRICATION

A conceptual drawing for spin-dependent transport along the out-of-plane direction in a FGF junction is shown in Fig. 1(a). Figures 1(b) and 1(c) show scanning electron microscopy (SEM) images of the side and top views, respectively, of the junction used in this study. The electrical spin transport properties of the junctions were obtained with the measurement configuration shown in Fig. 1(c). The sample fabrication procedure is illustrated in Figs. 2(a)–2(h). A clean oxidized Si substrate was first coated with a water-soluble poly (4-styrenesulfonic acid) (PSS) layer, which was subsequently coated with a liftoff resist layer (LOR; manufactured by MicroChem), a sacrificial supporting layer, as shown in Fig. 2(a). A graphene flake was mechanically exfoliated onto the prepared substrate. Py electrodes were used for out-of-plane spin injection. First, the bottom electrode was prepared [Fig. 2(b)] on graphene by electron-beam (e-beam) patterning with 950 K poly (methyl) methacrylate (PMMA) resist, electron-gun (e-gun) evaporation of Py/Au (30/5 nm), and liftoff, resulting in a lateral dimension of 1×20 μm^2 [Fig. 2(b)]. In the liftoff process, hot xylene (50 °C) was used to remove the PMMA resist, whereas the PSS and LOR layers remained stable against xylene. Using a handling frame,

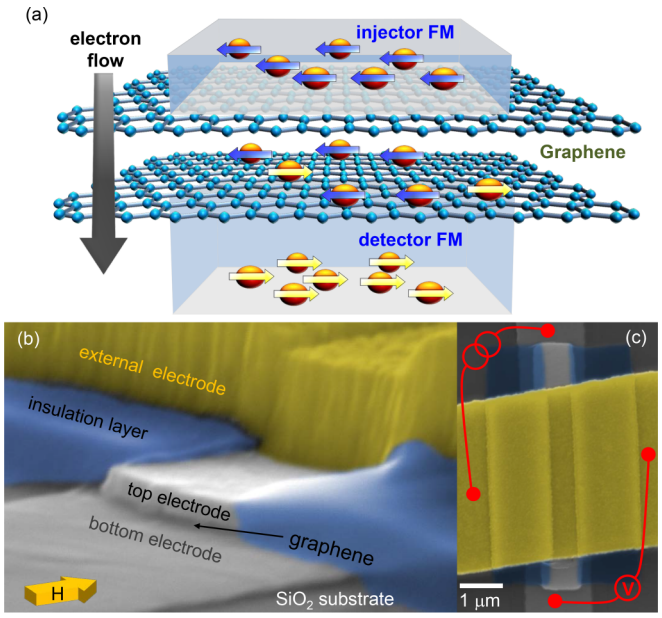

FIG. 1. (Color online) (a) A conceptual drawing for spin-dependent transport in a vertically stacked FGF junction. Scanning electron microscopy image of the junction. (b) Side view of the junction. (c) Top view of the junction with the measurement configuration shown.

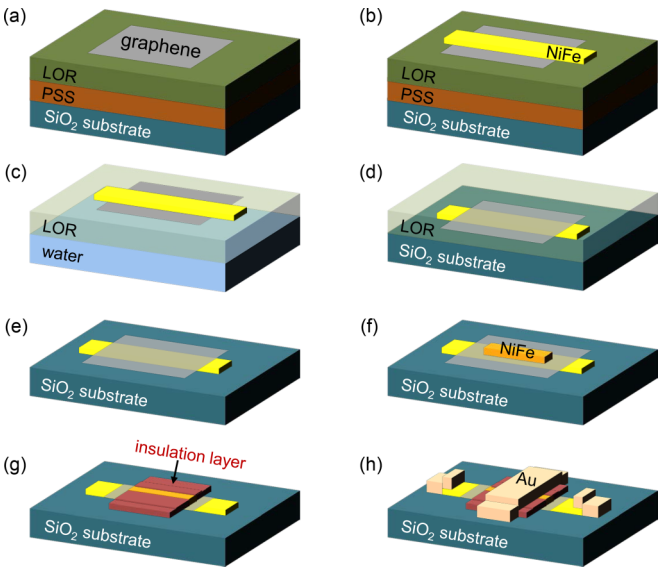

FIG. 2. (Color online) Sample fabrication processes. (a) Exfoliation of natural graphene on an oxidized Si substrate coated with a PSS/LOR layer. (b) Metal deposition (Py/Au; 30/5 nm) for the bottom electrode. (c) Dissolution of the PSS layer in water to separate the LOR layer from the Si substrate. (d) The LOR layer flipped onto a separate Si substrate. (e) Elimination of the LOR layer. (f) Metal deposition (Py/Au; 50/5 nm) for the top electrode. (g) Addition of an insulation layer with cross-linked PMMA. (h) Deposition of Au electrodes (Au; 250 nm).

we kept the entire substrate afloat on water. As the PSS layer dissolved in water, the LOR layer with the graphene/Py bilayer could be separated from the substrate [Fig. 2(c)]. The set of LOR−graphene/Py bilayers was flipped over onto a separate Si substrate, as shown in Fig. 2(d), followed by the removal of the LOR layer in a bath of hot Remover PG (manufactured by MicroChem) at 80 °C. After rinsing the sample consecutively in baths of isopropyl alcohol (IPA) and hexane, only a Py/graphene bilayer remained on the Si substrate [Fig. 2(e)]. During these processes, degradation of the graphene/Py interface from surface oxidation and chemical reaction of the Py electrodes was prevented by the gas impermeability of graphene [24–26]. In previous studies [19–21], the formation of an incomplete tunneling barrier due to oxidation of the bottom ferromagnetic electrodes may have induced spin-flip scattering [27,28]. The counter electrode, with the lateral dimensions listed in Table I, was prepared by additional e-gun evaporation of a Py/Au (50/5 nm) bilayer on graphene in alignment with the bottom electrode [Fig. 2(f)]. Then, the outer graphene layers were eliminated by O_2 plasma etching, except for the area of sandwiched graphene. The insulation layer was patterned using cross-linked 950 K PMMA resist (thickness: 200 nm), which was twice as thick as the total thickness of the bottom and top Py electrodes [Fig. 2(g)]. Finally, 250-nm-thick Au contact leads were deposited using e-gun evaporation [Fig. 2(h)]. The completed device was mounted onto a sample holder, which could be rotated with respect to the solenoid (or magnetic-field) direction and cooled down in a He^4 cryostat. The sample resistance was obtained by using a conventional lock-in technique (frequency: 13.33 Hz) with an alternating current (ac) bias current of $I = 50\ \mu$A (rms value) at $T = 4.2$ K.

III. RESULTS AND DISCUSSION

The junction parameters are summarized in Table I. We categorized the junctions into "transparent" and "resistive" junctions. The transparent junctions showed nonmetallic R-T curves with small $AR_{\rm cont}$, while the resistive junctions showed metallic R-T curves with large $AR_{\rm cont}$. The criterion for $AR_{\rm cont}$ separating the transparent and resistive junctions turned out to be $\sim 1\ \Omega\,\mu$m^2, which will be discussed in association with MR vs $AR_{\rm cont}$ curves.

Figures 3(a)–3(c) show the MR curves for FGF junctions with one, two, and four layers of graphene, respectively. Fixing the magnetic-field direction along the easy axis of Py electrodes, the magnetic field was swept first from +200 to −200 Oe (down sweeping), and then swept back to 200 Oe (up sweeping). The magnetization of the bottom and top FMs was first aligned parallel (P) to each other in the magnetic field of +200 Oe, yielding a low resistance. When the magnetic field was swept down, a transition occurred to an antiparallel (AP) configuration with high junction resistance due to the magnetization reversal of the softer FM of the two. An additional transition back to the P state took place near $-50 \sim -100$ Oe when the magnetization of the harder FM of the two was reversed. Similar magnetization-switching behavior with hysteresis was observed during the up-sweep of the magnetic field. In percent, the MR was defined by $[(R_{AP} - R_P)/R_P] \times 100$, where R_{AP} and R_P denote the

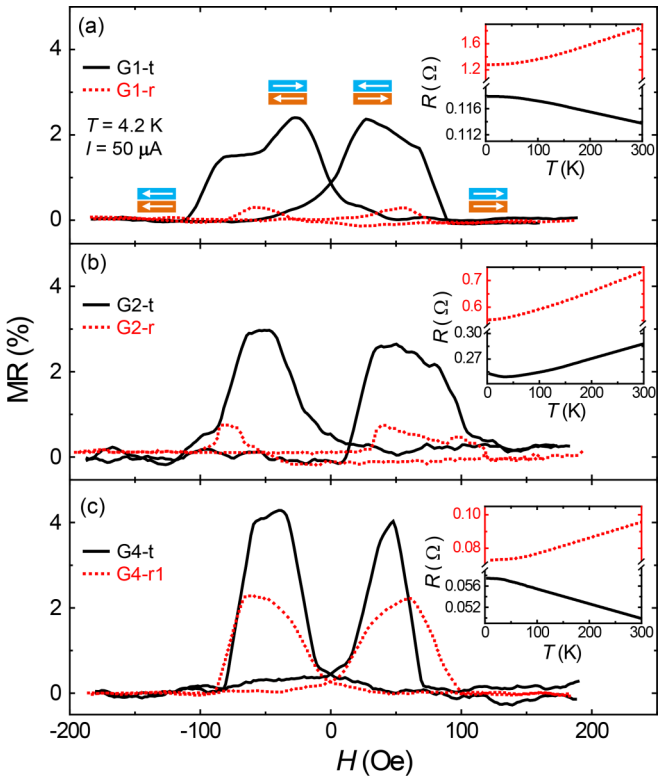

FIG. 3. (Color online) Comparison between transparent and resistive junctions. Hysteretic magnetoresistance (MR) curves for varying the magnetic field (H) at $T = 4.2$ K and $I = 50\ \mu$A for (a) G1-t and G1-r, (b) G2-t and G2-r, and (c) G4-t and G4-r1. Insets show the temperature dependence of the junction resistance for the corresponding samples with applied current $I = 50\ \mu$A. Transparent (G1-t, G2-t, and G4-t) and resistive (G1-r, G2-r, and G4-r1) junctions are denoted as solid and dotted lines, respectively.

resistance for the AP and P magnetization states between the two Py electrodes, respectively. Irregularity in the AP state may have originated from the presence of multiple domains at the bottom of the Py electrodes, built in during the e-gun evaporation process or caused by mechanical stress during the flip-transfer processes.

For each figure, comparison of the two sets of MR curves, both having an identical number of sandwiched graphene layers, revealed an obvious discrepancy in the magnitude of MR. This discrepancy largely depended on the magnitude of the junction resistance, as shown in the MR curves and their corresponding R-T curves. Comparing the MR with the junction resistance confirmed that higher (lower) MR was obtained in a FGF junction having smaller (larger) resistance. A detailed interpretation of the relationship between MR and the junction resistance is provided in the discussion below.

Another important feature in the R-T curves in the inset of Fig. 3 is the temperature variation of resistance in FGF junctions. For the transparent (resistive) junctions, the junction resistance increased (decreased) and then saturated with decreasing temperature, as denoted by the solid (dotted) lines, except for sample G2-t. The junction resistance of sample G2-t first decreased with decreasing temperature like the resistive junctions until the temperature reached ∼30 K. However,

below ∼30 K, the junction resistance increased slightly with decreasing temperature, similar to the transparent junctions. Because the MR measurements were made at 4.2 K, in the low-temperature range where an insulating R-T character appeared in the sample, sample G2-t was categorized as a transparent junction. Comparing these results with the expected out-of-plane resistance of a few mΩ in a single-layer graphene junction for the given dimensions in Table I, where the c-axis resistivity of the natural graphite was $\sim 10^{-3}$ Ω cm [29], most of the junction resistance occurred at the interface between the graphene and Py electrodes. The graphene/Py interface was expected to behave as an ohmic contact; this was confirmed by contact resistance measurements in Ni/graphene [30] and Pd/graphene [31] junctions.

In contrast, for the out-of-plane R-T measurements, nonmetallic behavior was observed in a few tens of nm thick graphite, both natural and highly ordered pyrolytic, whereas a metallic (nonmetallic) character was observed in natural (highly ordered pyrolytic) graphite thicker than a few μm [29,32,33]. Thus, it is clear that the metallic temperature dependence of junction resistance for the resistive junctions was dominated by the metallic but large contact resistance, whereas the nonmetallic junction resistance for the transparent junction was caused by the intrinsic out-of-plane resistivity of graphene. Thus, our transparent junctions exhibiting nonmetallic R-T curves better represent the intrinsic spin-dependent transport properties of FGF junctions with minimal interfacial scattering.

The temperature dependence of the maximum values of MR for samples G4-t, G2-t, G1-t, G4-r1, G3-r, and G4-r2, are illustrated in Fig. 4(a), from top to bottom, in the temperature range between 4.2 and 100 K. It is well known that the major factors contributing to temperature variation of MR in a metallic magnetic multilayer are phonon scattering and reduction of the mean-free path in the barrier [34–36]. In our FGF junctions, the MR decreased only slightly with increasing temperature. Linear fitting denoted by the solid lines in Fig. 4(a) exhibited a rate of change in MR with temperature in the range of $0.4 \sim 2.7 \times 10^{-3}$ %/K, which is one or two orders of magnitude smaller than that of magnetic multilayers [34] and spin-valve sandwiches [36]. In previous measurements on CVD-grown graphene insertion, similar rates of MR change with temperature were observed [19–21]. This weak variation of MR in our vertical FGF junctions was attributed to its metal-like character with weak electron-phonon coupling in graphene [37,38]. Weakly coupled graphene layers provide fewer scattering elements due to their relatively weak phonon vibration compared with normal metal insertion. Thus, the temperature variation of MR was weaker than that in normal metal-inserted magnetic multilayers.

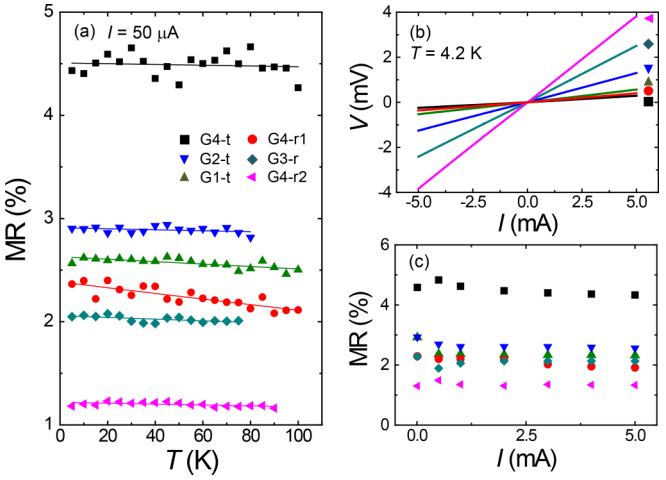

FIG. 4. (Color online) (a) Temperature dependence of MR for samples G4-t, G4-r1, G1-t, G2-t, G3-r, and G4-r2. Solid lines show the results for linear fitting. (b) I-V curves for the measured junctions. (c) Current bias dependence of MR for corresponding I-V curves. The same symbol legends are used for all figures.

Figure 4(b) shows the current-voltage (I-V) curves at $T = 4.2$ K. For all samples, including transparent junctions with nonmetallic R-T curves, the I-V characteristics were linear. The corresponding current-bias dependence of the MR is shown in Fig. 4(c). The MR values were retained even in the high-bias regime of $I \sim 5$ mA. In previous studies, nonlinear I-V curves and bias-dependent MR were observed in Ref. [19], where the MR decreased with increasing voltage bias, similar to that in magnetic tunnel junctions [39]. Linear I-V curves and bias-insensitive MR were observed in Refs. [20] and [21]. The linear I-V curves and the bias-insensitive MR over the entire bias range in this study confirmed that FGF graphene layers acted as metallic diffusive barriers along the out-of-plane direction rather than as a tunneling barrier formed by the degradation of the bottom electrodes. Furthermore, as shown in Table I, the extremely small $AR_{\rm cont}$ of our junctions, compared with the AR product in earlier studies of $35 \sim 75$ kΩ μm^2 [19], $40 \sim 100$ Ω μm^2 [20], and a few kΩ μm^2 [21], was attributed to the cleanness of the bottom-electrode surface. Because the high quality of the interface is crucial in spin-dependent transport, the passivation potential formed at the surface of few-layer graphene [24–26] improved the efficiency of the spin injection in our FGF junctions.

Figure 5 shows the interfacial-resistance dependence of MR for the FGF junctions used in this study. We defined interfacial resistance as $AR_{\rm cont} = A(R_{\rm jnc} - R_g)/2$, where A, $R_{\rm cont}$, $R_{\rm jnc}$, and R_g denote the junction area, contact resistance at the graphene/Py interfaces, total resistance of a FGF junction, and out-of-plane resistance of graphene, respectively. Here, we assumed identical $R_{\rm cont}$ values at both graphene/Py interfaces. Because R_g was two or three orders of magnitude smaller than $R_{\rm cont}$, R_g did not significantly affect the $AR_{\rm cont}$ value of FGF junctions. We adopted the functional relationship between the MR and $AR_{\rm cont}$ developed in Refs. [40–42] to obtain the spin asymmetry coefficients of the bulk (β) and interface (γ) from the MR for various FGF junctions. Here, β and γ correspond to the bulk magnetic polarization and the spin selectivity at the FM/nonmagnetic-metal interfaces, respectively. The estimated values of spin diffusion length in graphene [15] ($l_{sf}^N \simeq 100$ nm), out-of-plane resistivity of graphene [29] ($\rho_g \simeq 1 \times 10^{-3}$ Ω cm), and resistivity of Py [43] ($\rho_{\rm Py} \simeq 1.2 \times 10^{-5}$ Ω cm) led to pronounced MR in the range of the interfacial resistance, $AR_g(t_N/l_{sf}^N)$ ($\simeq 1 \times 10^{-5}$ Ω μm^2) $\ll AR_{\rm cont} \ll AR_g(l_{sf}^N/t_N)$ ($\simeq 1$ Ω μm^2), where t_N denotes the thickness of the graphene. Thus, as shown in Fig. 5, with increasing $AR_{\rm cont}$ passing the value 1 Ω μm^2,

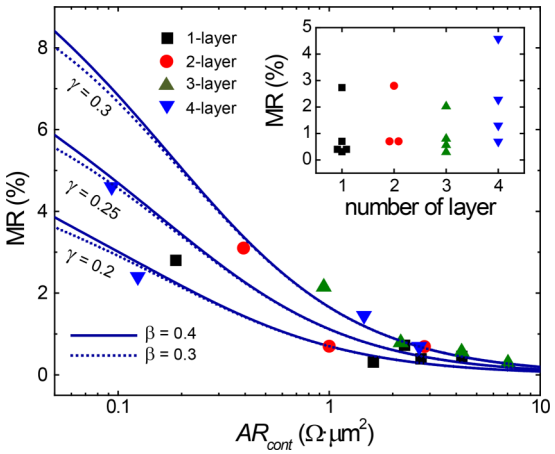

FIG. 5. (Color online) Interfacial resistance dependence of MR for various FGF junctions. Square, circle, upright-triangle, and inverted-triangle symbols indicate the MR for FGF junctions with one-, two-, three-, and four-layer graphene insertion, respectively. Best-fit curves are obtained for $\beta = 0.4$ (solid) and 0.3 (dotted) for three different values of γ: $\gamma = 0.3$ (upper), 0.25 (middle), and 0.2 (lower). We adopted estimated values of $l_{sf}^{N} \simeq 100$ nm, $\rho_g \simeq 1 \times 10^{-3}$ Ω cm, and $\rho_{\mathrm{Py}} \simeq 1.2 \times 10^{-5}$ Ω cm for the fit. The horizontal axis is plotted as a logarithmic scale of AR_{cont} for clarity. The inset shows the variation of MR for a different number of graphene layers.

MR slowly converged to zero. For $AR_{\mathrm{cont}} < 1$ $\Omega\,\mu\mathrm{m}^2$, the MR rapidly increased along with decreasing AR_{cont}, although the MR variation looks less steep in the semilogarithmic plot. The lower limit of pronounced MR [$AR_g(t_N/l_{sf}^{N}) \simeq 1 \times 10^{-5}$ $\Omega\,\mu\mathrm{m}^2$] were not in the measurement range of this study. Fit results indicated that our FGF junctions were in the regime of large AR_{cont} where $d(\mathrm{MR})/d(AR_{\mathrm{cont}})$ was negative. For both values of β (=0.3 and 0.4), curves with $\gamma = 0.25$ well fit the variation of MR with AR_{cont}. Values of $\gamma = 0.2$ and 0.3 provide the lower and upper bound of fits to the experimental results, respectively. It is clear that the graphene/Py interfaces in our FGF junctions acted as weak spin polarizers with $\gamma = 0.25 \pm 0.05$ compared with the value of the bulk polarization of the Py electrodes themselves, which is known to vary from 0.32 to 0.48 depending on the electrode preparation conditions [44].

In graphene consisting of weakly bonded multiple layers, the spin-polarized carriers were expected to propagate within the spin-flip length along the out-of-plane direction through sparsely distributed spin-scattering elements. Thus, the dominance of R_{cont} over R_g in total junction resistance is an obstacle to the effective spin injection and detection. Furthermore, the lower value of γ in our FGF junctions indicates that the reduction of the spin polarization of carriers occurred at the graphene/Py interfaces. A possible cause of the poor spin selectivity at the interfaces of FGF junctions was antiferromagnetic (AFM) ordering at the interfaces [45]. The antiparallel coupling at the FGF interfaces may have changed the spin polarization of injected carriers and led to low spin-injection efficiency at the interfaces of FGF junctions [46]. The stray magnetic field possibly induced by the corrugation of the graphene/Py interfaces also could have been the cause of lowering the interfacial spin selectivity in our devices [47].

In contrast to the theoretical prediction for perfect spin filtering through the interface between crystalline FM and graphene [12–14], the inset of Fig. 5 shows no clear correlation between the number of graphene layers and the observed MR. The spin filtering effect in our experiments may have been suppressed because the Py electrodes were polycrystalline or of alloy rather than single crystals, which resulted in the lower value of the interfacial spin-asymmetry coefficients $\gamma(=0.25 \pm 0.05)$. Opening of an exclusive band gap for the majority spins should be more rigorously examined, together with good control over the interfacial contact resistance between graphene and crystalline FM electrodes.

IV. CONCLUSION

Naturally stacked graphene layers having a varied number of atomic graphene sheets were adopted as an insert between two Py electrodes to form a FGF out-of-plane spin-valve junction. Passivation of Py electrodes by covering with graphene in association with direct electrode deposition onto graphene provided high-quality interfaces with a very small AR_{cont} in FGF junctions, as proven by the high MR up to 4.6% in a FGF junction consisting of four-layer graphene. The enhanced MR for more transparent interfaces indicates that the reduction of scattering at the graphene/Py interface raised the spin-injection efficiency in FGF junctions. However, fitting to a theoretical model suggests that the graphene/Py interfaces in our FGF junctions had an interfacial spin asymmetry coefficient of $\gamma(=0.25 \pm 0.05)$, which was much less than the value predicted theoretically for the spin-filtering effect. AFM ordering and the possible stray magnetic field at the interfaces of FGF junctions may have induced the suppressed spin polarization during transmission through graphene. The AFM-ordering effect could be reduced by inserting an additional nonmagnetic metal layer between graphene and the FMs, thus decoupling graphene from the FM [48–51]. Lattice matching between graphene and crystalline FMs [12–14] together with improved interfacial properties could also lead to significantly enhanced spin filtering.

ACKNOWLEDGMENTS

We are grateful for valuable discussion with Jonghwa Eom and Seung-Hyun Chun about vertical spin transport across graphene layers. This work was supported by the National Research Foundation (NRF) through the SRC Center for Topological Matter (Grant No. 2011-0030046) and the GFR Center for Advanced Soft Electronics (Grant No. 2011-0031640).

APPENDIX: FITTING EQUATION FOR VARIATION OF MR

We used a fitting function [Eqs. (A1) and (A2)] for MR variation as a function of interfacial resistance. These functions were proposed by Fert and Jaffrès [41] and used to obtain the curve fits in Fig. 5. In this model calculation, MR is defined by $\mathrm{MR} = \Delta R/R_P$ for a FM/normal-metal/FM

sandwiched structure along the out-of-plane direction. The areal resistance of a FM (normal-metal) electrode is defined by $r_{F(N)} = t_{F(N)}\rho_{F(N)}$, where $t_{F(N)}$ and $\rho_{F(N)}$ denote the thickness and resistivity of the FM (normal-metal), respectively. The quantity l_{sf}^{N} indicates the spin diffusion length of the normal metal and r_b^* is the interfacial resistance, adopted as AR_{cont} in this study:

$$\Delta R = \frac{2(\beta r_F + \gamma r_b^*)^2}{(r_b^* + r_F)\cosh\left(\frac{t_N}{l_{sf}^N}\right) + \frac{r_N}{2}\left[1 + \left(\frac{r_b^*}{r_N}\right)^2\right]\sinh\left(\frac{t_N}{l_{sf}^N}\right)}, \tag{A1}$$

$$R_P = 2(1-\beta^2)r_F + r_N\left(\frac{t_N}{l_{sf}^N}\right) + 2(1-\gamma^2)r_b^* + 2\frac{(\beta-\gamma)^2 r_F r_b^* + r_N(\beta^2 r_F + \gamma^2 r_b^*)\tanh\left(\frac{t_N}{2l_{sf}^N}\right)}{(r_b^* + r_F) + r_N\tanh\left(\frac{t_N}{2l_{sf}^N}\right)}. \tag{A2}$$

[1] I. Žutić, J. Fabian, and S. Das Sarma, Rev. Mod. Phys. **76**, 323 (2004).
[2] N. Tombros, C. Jozsa, M. Popinciuc, H. T. Jonkman, and B. J. van Wees, Nature (London) **448**, 571 (2007).
[3] W. Han and R. K. Kawakami, Phys. Rev. Lett. **107**, 047207 (2011).
[4] S. Jo, D.-K. Ki, D. Jeong, H.-J. Lee, and S. Kettemann, Phys. Rev. B **84**, 075453 (2011).
[5] D. Huertas-Hernando, F. Guinea, and A. Brataas, Phys. Rev. Lett. **103**, 146801 (2009).
[6] A. H. Castro Neto and F. Guinea, Phys. Rev. Lett. **103**, 026804 (2009).
[7] M. Gmitra, S. Konschuh, C. Ertler, C. Ambrosch-Draxl, and J. Fabian, Phys. Rev. B **80**, 235431 (2009).
[8] M. H. D. Guimarães, A. Veligura, P. J. Zomer, T. Maassen, I. J. Vera-Marun, N. Tombros, and B. J. van Wees, Nano Lett. **12**, 3512 (2012).
[9] I. Neumann, J. Van de Vondel, G. Bridoux, M. V. Costache, F. Alzina, C. M. S. Torres, and S. O. Valenzuela, Small **9**, 156 (2013).
[10] P. J. Zomer, M. H. D. Guimarães, N. Tombros, and B. J. van Wees, Phys. Rev. B **86**, 161416(R) (2012).
[11] T. Yamaguchi, Y. Inoue, S. Masubuchi, S. Morikawa, M. Onuki, K. Watanabe, T. Taniguchi, R. Moriya, and T. Machida, Appl. Phys. Express **6**, 073001 (2013).
[12] V. M. Karpan, G. Giovannetti, P. A. Khomyakov, M. Talanana, A. A. Starikov, M. Zwierzycki, J. van den Brink, G. Brocks, and P. J. Kelly, Phys. Rev. Lett. **99**, 176602 (2007).
[13] V. M. Karpan, P. A. Khomyakov, A. A. Starikov, G. Giovannetti, M. Zwierzycki, M. Talanana, G. Brocks, J. van den Brink, and P. J. Kelly, Phys. Rev. B **78**, 195419 (2008).
[14] J. Maassen, W. Ji, and H. Guo, Nano Lett. **11**, 151 (2010).
[15] T. Banerjee, W. G. van der Wiel, and R. Jansen, Phys. Rev. B **81**, 214409 (2010).
[16] Z. H. Xiong, D. Wu, Z. Valy Vardeny, and J. Shi, Nature (London) **427**, 821 (2004).
[17] J. H. Shim, K. V. Raman, Y. J. Park, T. S. Santos, G. X. Miao, B. Satpati, and J. S. Moodera, Phys. Rev. Lett. **100**, 226603 (2008).
[18] C. Barraud, P. Seneor, R. Mattana, S. Fusil, K. Bouzehouane, C. Deranlot, P. Graziosi, L. Hueso, I. Bergenti, V. Dediu, F. Petroff, and A. Fert, Nat. Phys. **6**, 615 (2010).
[19] E. Cobas, A. L. Friedman, O. M. J. vant Erve, J. T. Robinson, and B. T. Jonker, Nano Lett. **12**, 3000 (2012).
[20] M. Iqbal, M. W. Iqbal, J. H. Lee, Y. S. Kim, S.-H. Chun, and J. Eom, Nano Res. **6**, 373 (2013).
[21] J.-J. Chen, J. Meng, Y.-B. Zhou, H.-C. Wu, Y.-Q. Bie, Z.-M. Liao, and D.-P. Yu, Nat. Commun. **4**, 1921 (2013).
[22] B. Dlubak, M.-B. Martin, R. S. Weatherup, H. Yang, C. Deranlot, R. Blume, R. Schloegl, A. Fert, A. Anane, S. Hofmann, P. Seneor, and J. Robertson, ACS Nano **6**, 10930 (2012).
[23] G.-H. Lee and H.-J. Lee, Appl. Phys. Express **6**, 025102 (2013).
[24] J. S. Bunch, S. S. Verbridge, J. S. Alden, A. M. van der Zande, J. M. Parpia, H. G. Craighead, and P. L. McEuen, Nano Lett. **8**, 2458 (2008).
[25] Y. S. Dedkov, M. Fonin, and C. Laubschat, Appl. Phys. Lett. **92**, 052506 (2008).
[26] S. Chen, L. Brown, M. Levendorf, W. Cai, S.-Y. Ju, J. Edgeworth, X. Li, C. Magnuson, A. Velamakanni, R. D. Piner, J. Kang, J. Park, and R. S. Ruoff, ACS Nano **5**, 1321 (2011).
[27] E. Y. Tsymbal, A. Sokolov, I. F. Sabirianov, and B. Doudin, Phys. Rev. Lett. **90**, 186602 (2003).
[28] S. Maekawa and U. Gäfvert, IEEE Trans. Magn. **18**, 707 (1982).
[29] K. Matsubara, K. Sugihara, and T. Tsuzuku, Phys. Rev. B **41**, 969 (1990).
[30] A. Venugopal, L. Colombo, and E. M. Vogel, Appl. Phys. Lett. **96**, 013512 (2010).
[31] F. Xia, V. Perebeinos, Y.-m. Lin, Y. Wu, and P. Avouris, Nat. Nanotechnol. **6**, 179 (2011).
[32] W. Prismak and L. H. Fuchs, Phys. Rev. **95**, 22 (1954).
[33] L. Casparis, D. Hug, D. Kölbl, and D. M. Zumbühl, arXiv:1301.2727.
[34] F. Petroff, A. Barthélémy, A. Hamzić, A. Fert, P. Etienne, S. Lequien, and G. Creuzet, J. Magn. Magn. Mater. **93**, 95 (1991).
[35] S. S. P. Parkin, Z. G. Li, and D. J. Smith, Appl. Phys. Lett. **58**, 2710 (1991).
[36] B. Dieny, P. Humbert, V. S. Speriosu, S. Metin, B. A. Gurney, P. Baumgart, and H. Lefakis, Phys. Rev. B **45**, 806 (1992).
[37] K. I. Bolotin, K. J. Sikes, J. Hone, H. L. Stormer, and P. Kim, Phys. Rev. Lett. **101**, 096802 (2008).
[38] E. H. Hwang and S. Das Sarma, Phys. Rev. B **77**, 115449 (2008).
[39] M. Julliere, Phys. Lett. A **54**, 225 (1975).
[40] T. Valet and A. Fert, Phys. Rev. B **48**, 7099 (1993).
[41] A. Fert and H. Jaffrès, Phys. Rev. B **64**, 184420 (2001).

[42] S. S. P. Parkin, A. Modak, and D. J. Smith, Phys. Rev. B **47**, 9136 (1993).
[43] S. B. Kumar, M. B. A. Jalil, S. G. Tan, and Z. Y. Leong, Phys. Rev. B **74**, 184426 (2006).
[44] J. S. Moodera and G. Mathon, J. Magn. Magn. Mater. **200**, 248 (1999).
[45] B. Li, L. Chen, and X. Pan, Appl. Phys. Lett. **98**, 133111 (2011).
[46] J. M. De Teresa, Physics **2**, 13 (2009).
[47] P. K. Muduli, J. Barzola-Quiquia, S. Dusari, A. Ballestar, F. Bern, W. Böhlmann, and P. Esquinazi, Nanotechnology **24**, 015703 (2013).
[48] A. Nagashima, N. Tejima, and C. Oshima, Phys. Rev. B **50**, 17487 (1994).
[49] Y. S. Dedkov, A. M. Shikin, V. K. Adamchuk, S. L. Molodtsov, C. Laubschat, A. Bauer, and G. Kaindl, Phys. Rev. B **64**, 035405 (2001).
[50] A. Varykhalov, D. Marchenko, J. Sánchez-Barriga, M. R. Scholz, B. Verberck, B. Trauzettel, T. O. Wehling, C. Carbone, and O. Rader, Phys. Rev. X **2**, 041017 (2012).
[51] A. A. Rybkina, A. G. Rybkin, V. K. Adamchuk, D. Marchenko, A. Varykhalov, J. Sánchez-Barriga, and A. M. Shikin, Nanotechnology **24**, 295201 (2013).